Mineralium Deposita
https://doi.org/10.1007/s00126-024-01333-9

ARTICLE

Coupled antimony and sulfur isotopic composition of stibnite as a window to the origin of Sb mineralization in epithermal systems (examples from the Kremnica and Zlatá Baňa deposits, Slovakia)

Peter Koděra[1] · Ryan Mathur[2] · Degao Zhai[3] · Rastislav Milovský[4] · Pavel Bačo[5] · Juraj Majzlan[6]

Received: 13 February 2024 / Accepted: 30 October 2024

Abstract

Stibnite is a relatively common mineral in epithermal deposits, with little known about Sb transport and efficient stibnite precipitation. The famous Kremnica Au-Ag low-sulfidation deposit and Zlatá Baňa intermediate-sulfidation Pb-Zn-Cu-Au-Ag-Sb deposit are hosted in two different Neogene volcanic fields in Western Carpathians, Slovakia. In both deposits, stibnite-rich veins occur outside of major vein structures, accompanied by illite, illite/smectite, and kaolinite alteration, and affiliated to late-stage fluids (< 2 wt% NaCl eq., < 150 °C). Sulfur isotopic composition of stibnite and sulfides is different at both deposits, likely due to a different magmatic-hydrothermal evolution of the parental magmatic chambers in the Central and Eastern Slovak Volcanic Fields. The Sb isotopes (δ^{123}Sb), however, show similar values and trends of gradual simultaneous increase with δ^{34}S values, explained by a progressive precipitation of stibnite and its fractionation with the fluid. The data were modeled by two coupled Rayleigh fractionation models, (for Sb and for S), assuming a predominant Sb transport in $HSb_2S_4^-$ with a variable amount of S species. Higher molality ratio m_S/m_{Sb} of fluids was found in Kremnica (~ 3–4) than in Zlatá Baňa (~ 2). At both deposits, the heaviest δ^{123}Sb values are accompanied by a decrease in the δ^{34}S values probably due to the commencement of pyrite/marcasite precipitation. According to thermodynamic models of solubility of Sb(III) complexes and observations from active geothermal fields, stibnite precipitation was triggered by temperature decrease accompanied by mixing with a mildly acidic fluid (pH 4–5) of a steam-heated CO_2-rich condensate on margins and in the final stages of epithermal systems. The proposed model for the origin of stibnite-bearing veins in epithermal systems can be used for their better targeting and efficient mineral exploration.

Keywords Antimony · Stibnite · Epithermal · Genesis · Sulfur · Isotope

Editorial handling: M. Gadd

✉ Peter Koděra
peter.kodera@uniba.sk

[1] Department of Mineralogy, Petrology and Economic Geology, Faculty of Natural Sciences, Comenius University, Ilkovičova 6, Bratislava 842 15, Slovakia

[2] Department of Geology, Juniata College, Huntingdon, PA 16652, USA

[3] State Key Laboratory of Geological Processes and Mineral Resources, China University of Geosciences, Beijing, China

[4] Earth Science Institute, Slovak Academy of Sciences, Ďumbierska 1, Banská Bystrica 974 11 , Slovakia

[5] State Geological Institute of Dionýz Štúr, Jesenského 8, Košice 040 01, Slovakia

[6] Institut für Geowissenschaften, Friedrich-Schiller, Universität Jena, Carl-Zeiss-Promenade 10, Mineralogie, Jena D- 07745, Germany

Introduction

Stibnite mineralization in epithermal systems is relatively common, however, they rarely form economic accumulations. They are present in volcanic belts of active continental margins formed in subsurface conditions with high geothermal gradients (up to 30–35 °C/100 m; Obolensky et al. 2007). They commonly occur in peripheral portions of the epithermal systems (e.g., on the top of an Au-Ag orebody near the surface) or overprint Au-Ag mineralization at depth (Morteani et al. 2011; Schwarz-Schampera 2014; Shimizu 2017). An example of the latter case is the Hishikari Au-Ag deposit in Japan, where stibnite occurs within the bonanza zone and overprints the Au-Ag mineralization at the same depth. In the Neogene volcanic arc of Carpathians, there are also several examples of the presence of stibnite in precious and base-metal epithermal veins in Romania (e.g., Baia

Published online: 26 December 2024

Sprie, Capnik), Hungary (Gyöngyösoroszi), and Slovakia (Kremnica, Zlatá Baňa) (Böhmer 1980; Veľký et al. 1998). The Slovak deposits were mined, among other commodities, also for Sb. However, the behavior of antimony in natural epithermal systems is not well understood, in contrast to much more extensive knowledge of the transport and deposition of Au, Ag, Pb, Zn, and Cu (e.g., Corbett and Leach 1998; Hedenquist et al. 2000; Simmons et al. 2005; Wang et al. 2019). Antimony is recognized as a critical raw material/mineral in the EU, the US, Japan and Australia, thus improved knowledge on genesis of antimony in epithermal systems can be used in more efficient exploration of this commodity worldwide.

Stibnite is sometimes present in geothermal systems, which unlike most other hydrothermal systems, can be studied directly in situ. Some of them are exploited as sources of geothermal energy and were documented to precipitate gold or galena (e.g., Wilson et al. 2007; Simmons et al. 2016; Ledésert et al. 2021) upon temperature decrease of fluids. Stibnite precipitation also occurs in geothermal wells, such as those in Tuscany power plants in Italy (Morteani et al. 2011). This power station operates at roughly 200 °C, thus the scales form at above 200 °C. Morteani et al. (2011) showed experimentally that depressurization separates Sb and As into the liquid phase and Hg into the gas phase. This separation explains the often-observed areal separation of Hg and Sb mineralization. Furthermore, the authors found that metastibnite is the first Sb_2S_3 modification to crystallize in the scales of the geothermal wells together with amorphous silica, while in the second stage, the opaline groundmass undergoes dehydration and metastibnite transforms to stibnite. The authors argue that this may explain the differences in fluid inclusion data between inclusions in apparently coeval stibnite and quartz as observed from fluid inclusion studies of some stibnite deposits (e.g., Hagemman and Lüders 2003; Majzlan et al. 2020). This includes fluid inclusion data on Sb (Au) mineralization from the Tuscany region, having wide range of temperatures from 245 to 115 °C (Tanelli et al. 1991).

Not all mineralogical, geochemical, and textural features of such systems can be explained by the short-term observations at the geothermal plants, though. One of the poorly known parameters of such systems is the timing and frequency of metal supply and delivery from the source, usually a magmatic chamber and/or surrounding rocks. Banded textures of bonanza gold ores in epithermal systems, with alternating bands of chalcedony and ore minerals (Izawa et al. 1990; Saunders et al. 2008; Shimizu 2014; Tharalson et al. 2023), suggest that precipitation and deposition is repeated and episodic. It is not clear, though, if the episodic nature of deposition means also episodic nature of metal supply. These authors point out that the frequent textural changes in gold mineralization can be assigned to variable degree of boiling in such systems, from vigorous to mild and to non-boiling conditions. However, precipitation of stibnite in epithermal systems is probably rarely repeated and episodic as it occurs usually in final stages of mineralization (e.g., Schwarz-Schampera 2014; Shimizu 2017). Furthermore, cooling and/or acidification is probably the most frequent trigger for precipitation of stibnite, as seen on data from geothermal fields (Wilson et al. 2007; Morteani et al. 2011) but boiling of ore fluids is sometimes also proposed to control the stibnite precipitation along with their cooling (Yu et al. 2023). Although stibnite is commonly formed in epithermal gold deposits, its genesis, including transport mechanism, may be different and needs further investigation.

Research on stable isotopes of antimony (^{121}Sb and ^{123}Sb) is a relatively new geochemical field that can be used as a process tracer in hydrothermal ore deposits containing Sb minerals. Antimony isotopes display a natural variation of $\delta^{123}Sb$ values of around 2‰. The processes that are responsible for isotopic variations include redox reactions, biological processes, evaporation and precipitation processes, adsorption, and Rayleigh distillation mechanisms (Tanimizu et al. 2011; Wen et al. 2018; Wasserman et al. 2019; Zhou et al. 2022, 2023). Zhai et al. (2021) demonstrated that ore fluids are preferentially enriched in heavier Sb isotopes during the precipitation of isotopically lighter stibnite that could be used to fingerprint hydrothermal fluid flow in a closed system. They estimated the Sb isotope fractionation factor as $\alpha_{fluid-stibnite} = 0.9994$. A similar trend of Sb isotope fractionation was recorded in an assemblage of hydrothermal Sb minerals, not only stibnite (Kaufmann et al. 2023). A comparable fractionation of 0.9‰ occurs during reduction processes from Sb^{5+} to $Sb^{3}+$ (Rouxel et al. 2003). Wang et al. (2021) discussed the redox-controlled Sb isotope fractionation in an epithermal system, whereas Yu et al. (2022) showed the effect of the Sb speciation change in the fluid on Sb isotopic fractionation. The potential of Sb isotopes to trace the preferential complexing of Sb in hydrothermal fluids and implications for fluid evolution and stibnite precipitation mechanism was recently presented by Yu et al. (2023).

In this work, we investigated the isotopic changes of Sb and S in stibnite mineralization at two epithermal deposits in the Western Carpathians, at Kremnica and Zlatá Baňa, hosted by two different Neogene volcanic fields (Fig. 1). Systematic and comparable trends in both isotopic systems at these two deposits witness the processes associated with Sb and S delivery and precipitation of metallic and non-metallic minerals. In this contribution, we present the results of modelling that enabled to reproduce the behavior of Sb and S isotopes in studied epithermal systems and to track down the processes that led to Sb delivery and stibnite precipitation in epithermal systems.

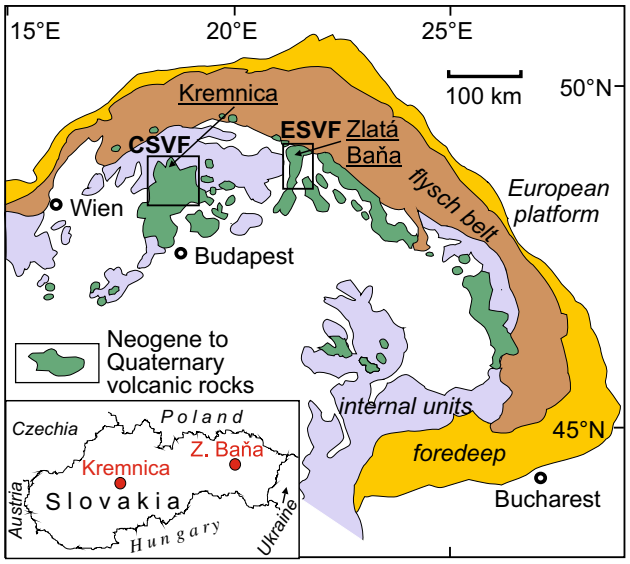

Fig. 1 Regional geological setting of the two studied deposits, Kremnica and Zlatá Baňa, in the Central Slovak Volcanic Field (CSVF) and the Eastern Slovak Volcanic Field (ESVF), respectively, among the Neogene to Quaternary volcanic rocks of the Carpathian arc and the Pannonian basin (after Lexa et al. 1999). Inset shows location of the deposits in Slovakia among geopolitical boundaries

Stibnite mineralization in the Kremnica Au-Ag epithermal deposit

Geological setting

The Kremnica Au-Ag deposit is located in the northern part of the Neogene Central Slovak Volcanic Field (CSVF) in the Kremnické Vrchy mountain range. Main volcanic rocks include remnants of a large andesite stratovolcano with subvolcanic intrusive rocks in the central zone, a N-S trending graben with volcanic formations including variably differentiated andesitic rocks over 1000 m in thickness, remnants of 4 younger volcanoes situated next to marginal faults of the graben, and a resurgent horst in the central part of the graben associated with a late-stage rhyolite magmatic activity (Lexa et al. 1998).

The resurgent horst is built by the pre-graben propylitized andesite complex. The horst is surrounded by andesitic rocks of graben fill (15.0-13.5 Ma; Lexa et al. 1998). Eastern marginal faults of the horst host an extensive epithermal vein system, including the Kremnica Au-Ag deposit (Fig. 2A). The structure of the horst is dominated by N-S and NE-SW trending normal faults, corresponding to the

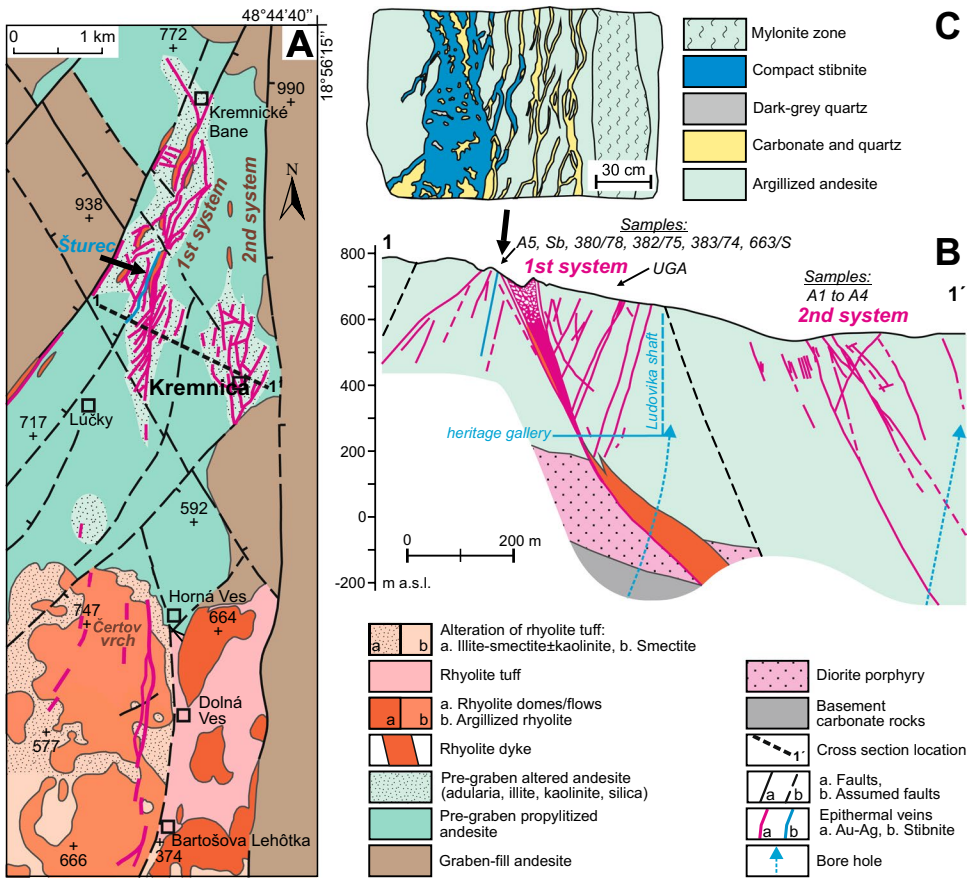

Fig. 2 Geological setting of stibnite mineralization in the Kremnica Au-Ag ± Sb epithermal deposit, including distribution of Sb ore veins and hydrothermal alteration. **a** Simplified structural scheme of resurgent horst hosting the deposit (after Kraus et al. 1994; Finka 2009). **b** Cross section of the central part of the deposit including the position of studied samples (after Böhmer and Škvarka 1970; Veľký et al. 1998). **c** Sketch of the mine face with stibnite ore in the Václav adit in Šturec with its position in the section pointed by arrow in A and B. (redrawn after Korim in Veľký et al. 1998)

regional stress field with strong NW-SE extension during the interval 13.5-9.0 Ma (Nemčok et al. 1993). According to Kraus et al. (1999) and Pécskay et al. (2010), uplift of the horst was contemporaneous with the epithermal mineralization (11.1–10.1 Ma on illite, 12.1–11.5 Ma on adularia) and emplacement of the products of rhyolite magmatic activity (12.3–11.5 Ma).

Epithermal mineralization

The Kremnica gold deposit was one of the most important gold producers in the Medieval Europe with at least one thousand years of mining history (Bakos et al. 2004; Finka 2009), considerable historical production of precious metals (~46 t Au and 208 t Ag; Finka 2009) and 25 Mt of ore reserves with 1.42 g/t Au (www.ortacresources.com). More than 120 veins are known within this deposit. They are mostly hosted by the pre-graben andesite and the principal characteristics of the deposit are indicative of epithermal mineralization of low-sulfidation style (Koděra et al. 2014).

The veins are grouped into two major vein systems (Fig. 2A and B). The first one consists of veins that are hosted by a first-order listric transtension/extension fault accompanied by low-angle second-order vein structures close to the surface, and complementary antithetic veins. The vertical extent of the mineralized fault exceeds 1200 m, with a dip of 50°-60°. The fault gradually opens towards the surface to its maximum width of 80 m in the central part at Šturec. Some of these faults are intruded by rhyolite dikes. The second vein system is located in the hanging wall of the master listric fault, underneath the Kremnica town (Koděra et al. 2007).

Only the upper 200–300 m parts of veins are enriched in precious metals, while the ore grades usually vary over the range of 1–5 g/t Au and 5–30 g/t Ag (Böhmer 1966; Böhmer et al. 1977; Veľký et al. 1998; Bartalský and Finka 1999). Vein filling is represented by banded and cavernous quartz, occasionally with carbonates. Mineralogical studies determined two major ore stages (Au-Ag and Sb-Hg stage), with 6 sub-stages (Fig. 3; Böhmer 1966; Veľký et al. 1998). The Au-Ag stage contains early minor barren carbonate sub-stage (1), two quartz sub-stages (2 and 3) and pyrite sub-stage (4). Microscopic Au precipitated mostly during the pyrite sub-stage and occurs as electrum or gold in pyrite and quartz in dark quartz-chalcedony bands with finely dispersed pyrite/marcasite. In the 2nd vein system, gold is also present in rare visible aggregates up to 7 cm long (Bakos et al. 2004). In both vein systems, pyrite and arsenopyrite are the most common ore minerals, accompanied by minor galena, sphalerite, chalcopyrite, proustite, pyrargyrite, and Ag sulfosalts.

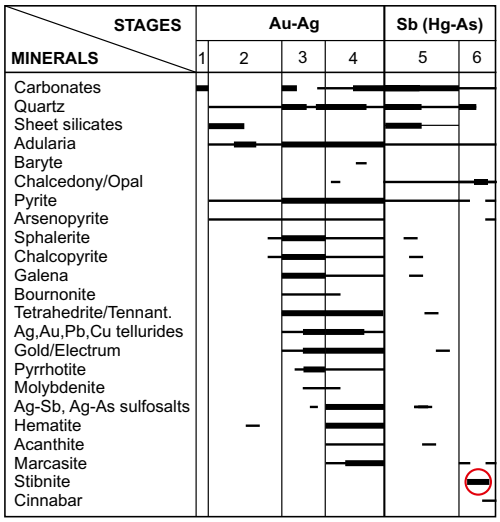

Fig. 3 Simplified paragenetic scheme of the Kremnica epithermal deposit with highlighted position of stibnite precipitation. The individual sub-stages, delineated in the diagram by vertical lines, are separated by intermineralization tectonics. The line thickness corresponds to the mineral abundance in the veins. After Böhmer (1966) and Veľký et al. (1998)

The Sb ± Hg, As stage followed after intensive intermineralization tectonics, including dislocations of products of the earlier stage (Böhmer 1966; Veľký et al. 1998). It fills mainly fissures, especially in the hanging wall of the major vein structure. This stage includes quartz-carbonate sub-stage (5) with predominant dolomite and minor quartz with rare, disseminated sulfides, sulfosalts, and electrum. Carbonates prevail especially in the upper and outermost parts of veins. Stibnite sub-stage (6) with common stibnite, pyrite, marcasite in a quartz-chalcedony gangue is best developed in the footwall structures (mainly at Šturec, Fig. 2B and C).

Extensive wall-rock alteration includes adularia, quartz, illite, kaolinite, passing outwards into illite/smectite (I/S), kaolinite, chlorite, smectite, variably with disseminated pyrite and carbonate (Böhmer 1966; Kraus et al. 1994). Kaolinite is especially common close to the surface (down to 100–200 m), in veins and in the wall rocks (Böhmer et al. 1969). Kaolinite is indicative for the formation of large areas of steam-heated low-pH aqueous fluids that accompanied the veins at subsurface level. Acid alteration resulted from condensation of H_2S and CO_2-bearing vapor released during boiling, which was documented by fluid inclusion data. The steam-heated origin of kaolinite from vein wall-rock alteration at temperatures ~ 50–90 °C was confirmed by oxygen and hydrogen isotopic studies (Koděra et al. 2014).

Stibnite mineralization

According to the works of Böhmer (1980) and (Finka 2009) mineralization of the Sb ± Hg, As stage fills fissures nearly exclusively outside of the major vein structures in the 1st vein system hosted by the pre-graben andesite. It occurs in their hanging wall, but especially in their footwall mainly in the central part at Šturec, forming steep antitethic veins of the Schrämen vein (Fig. 2B). These veins are about 300 m long and 0.5 to 2 m thick, containing 3% Sb in average. From these veins, 25.8 kt of Sb ores were exploited in the years 1971–1972 on the level of the Václav adit. In the 2nd vein system, stibnite crystals occur in cavities of earlier precious metal mineralization, accompanied by minor dark opal. Minor stibnite mineralization is also present in the northern part of the vein system (Hlavná, Kirchberg veins) and in the southern part of the vein system hosted by rhyolite (Horná Ves, Bartošova Lehôtka) (Böhmer 1980; Finka 2009).

Based on the studies of Böhmer (1966) and Veľký et al. (1998), stibnite mineralization forms veinlets, metasomatic bodies and disseminated stockworks with common stibnite, pyrite, and marcasite. The veins include both quartz-carbonate (5) and later stibnite sub-stages (6), divided by a minor local inter-mineralization tectonics between these sub-stages (Figs. 2C and 3). Carbonates prevail in the quartz-carbonate sub-stage and consist of Fe-rich dolomite to ankerite. Stibnite often forms euhedral crystals, sometimes up to 10 cm long, but also occurs in massive or disseminated forms and replaces carbonates of the earlier sub-stage (Fig. 2C). It has increased Hg content (Böhmer 1980). Quartz is often dark due to fine disseminations of pyrite and stibnite. Minor pyrite is mostly earlier than stibnite while marcasite is commonly later, forming coatings and crusts in cavities. Rare arsenopyrite and opal are also sometimes present. Antimony content decreases in deeper parts and stibnite ore is replaced by marcasite mineralization (Böhmer 1966, 1980; Veľký et al. 1998). Böhmer (1980) argued that the most extensive precipitation of stibnite occurred in the vicinity of a thick impermeable zone of mylonitized andesite in the footwall of the Schrämen vein (Fig. 2C).

Stibnite mineralization in the Zlatá Baňa epithermal deposit

Geological setting

The Zlatá Baňa Pb-Zn-Au-Ag-Sb deposit is located in the northern part of the Neogene Eastern Slovak Volcanic Field (ESVF) in the Slanské Vrchy Mountains. The deposit is

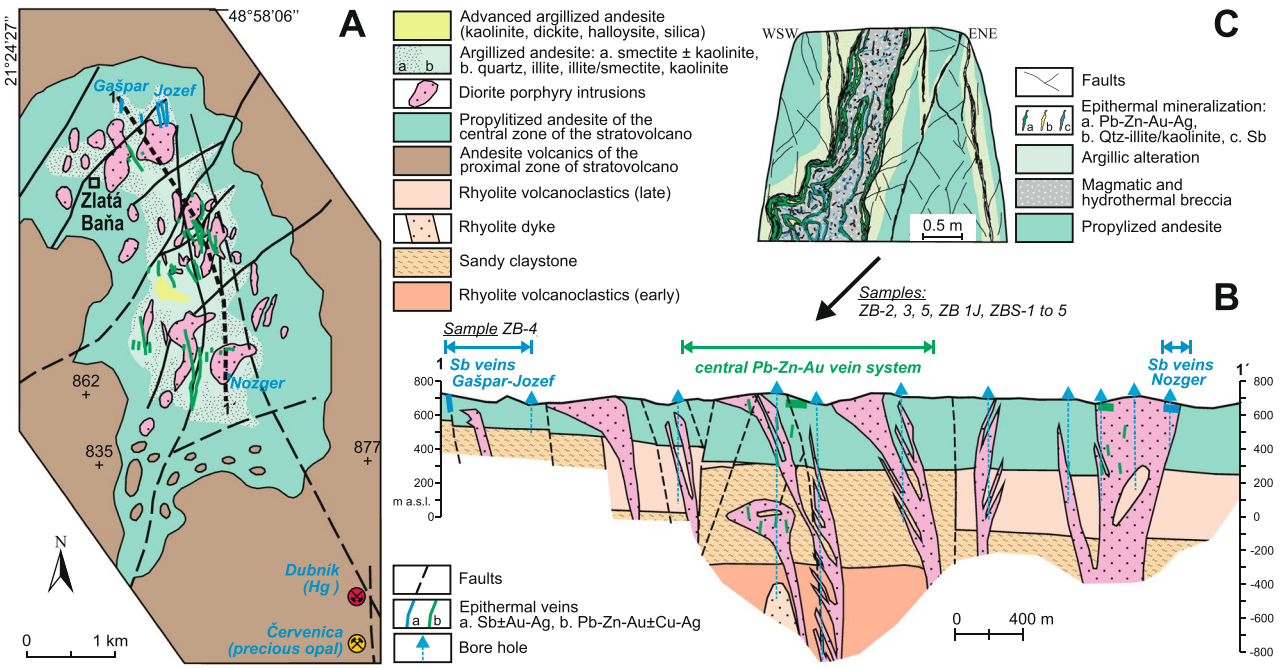

Fig. 4 Geological setting of stibnite mineralization in the Zlatá Baňa Pb-Zn-Cu-Au-Ag-Sb epithermal deposit, including distribution of Sb ore veins and hydrothermal alteration. **a** Simplified structural scheme of the central zone of the Zlatá Baňa stratovolcano (after Divinec et al. 1988; Kaličiak et al. 1991b; Štohl et al. 1994; Molnár et al. 2010). **b** Cross section of the central zone of the stratovolcano along the line 1–1', showing the spatial relationship of stibnite-rich and polymetallic veins and the position of studied samples (modified from Divinec et al. 1988). Note that the direction of most of the veins is along the profile which results in their limited visibility in the profile. **c** Sketch of the mine face with polymetallic ore, including late stibnite mineralization in the adit "3" in the central part of the deposit, with its position in the section pointed by arrow (modified from Bačo and Repčiak in Lexa et al. 2002)

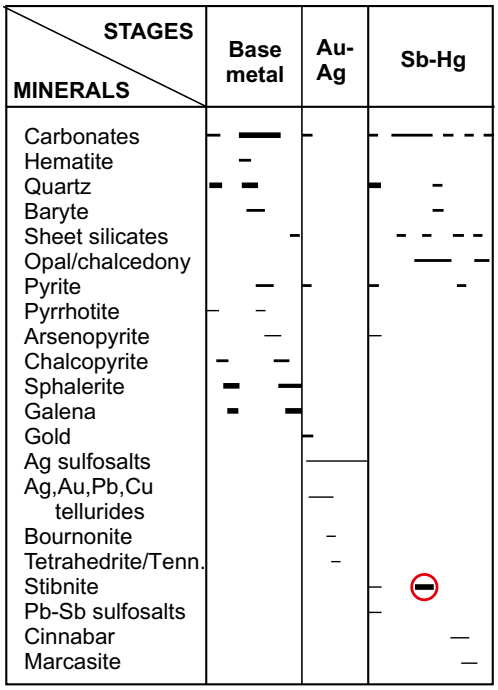

Fig. 5 Simplified paragenetic scheme of the Zlatá Baňa epithermal deposit with highlighted position of stibnite precipitation. The individual stages, delineated in the diagram by vertical lines, are separated by intermineralization tectonics. The line thickness corresponds to the mineral abundance in the veins, broken lines represent the occurrence of a mineral in multiple substages. After Ďuďa (1992), Chovan et al. (1994) and Lexa et al. (2002)

hosted by the central zone of the Zlatá Baňa andesite stratovolcano (12.2–10.0 Ma), located in the northern part of the Slanské Vrchy Mts and mostly built by an extensive effusive andesite complex (Kaličiak and Repčok 1987; Štohl et al. 1994). The central zone of the stratovolcano contains effusive, extrusive, and intrusive bodies of pyroxene andesite and diorite porphyry (Fig. 4A and B). The porphyry intrusions contain minor disseminated stockwork Cu-mineralization at depth, accompanied by K-metasomatic alteration with secondary biotite. This zone is represented by a marked cauldron-shaped depression that has a complicated horst-graben structure, segmented by a system of NE-SW and NW-SE faults (Kaličiak et al. 1991a; Molnár et al. 2010).

Epithermal mineralization

Epithermal vein mineralization is hosted by altered andesite and diorite porphyry in the central zone of the stratovolcano (Fig. 4A and B). According to mineralogical studies of Kaličiak and Ďuďa (1981), Kovalenker et al. (1988) and Ďuďa (1992), three main stages of epithermal mineralization can be distinguished in the central zone: base metal, Au-Ag and Sb-Hg stage (Fig. 5). The middle part of the volcanic structure hosts predominantly veins and stockworks containing Pb-Zn-Au ± Cu-Ag mineralization, while in the marginal parts there occur younger Sb ± Au-Ag and Sb ± Hg ores (Fig. 4). The base-metal veins have NNW–SSE to N–S direction and are steeply dipping to E as well as W. South of the central zone, in the less eroded proximal zone of the volcano, disseminated Hg-Sb-As and precious-opal mineralizations are present (Hg deposit Dubník, precious-opal deposit Červenica, Fig. 4A). The Sb-Au-Ag veins were mined since the 17th century until the early 20th century (Kaličiak and Ďuďa 1981; Bačo in Lexa et al. 2002; Molnár et al. 2010).

The vein thickness is highly variable, ranging from 0.1 to 5.2 m (average 1.1 m). The main ore minerals of base-metal veins are pyrite, sphalerite, galena, and chalcopyrite (Fig. 5). The precious-metal mineralization, with average grades 1.4 g/t Au and 39.7 g/t Ag, is superimposed on the base-metal ores and is concentrated in the near-surface parts of veins. It consists of native Au, electrum, native Ag, petzite, hessite, acanthite, polybasite, miargyrite, and numerous rare Ag-Pb-Sb sulfosalts (Fig. 5). The gangue of both types of mineralizations consists of carbonates and quartz (Kaličiak and Ďuďa 1981; Divinec et al. 1988; Ďuďa 1992; Bačo in Lexa et al. 2002).

Veins, stockworks, and hydrothermal breccias are accompanied by illite alteration, which has regional distribution in the central part of the volcanic structure, passing outwards to smectite alteration and the outermost propylitization with chlorite, calcite, and pyrite (Fig. 4A). The wall rock alteration locally overlaps with advanced argillic alteration (kaolinite, dickite, halloysite, residual silica) related to the porphyry intrusions (Bačo in Lexa et al. 2002; Molnár et al. 2010).

Stibnite mineralization

Stibnite belongs to the latest stage of mineralization, postdating both the base-metal and Au-Ag mineralization, which occupy the same vein structures. There are three stibnite-bearing veins in the northern margin (Gašpar and Jozef Sb ± Au-Ag veins) and one vein in the southern margin of the central zone (Nozger Sb ± Hg veins), in which the Sb-bearing mineralization spatially overlaps with the earlier base-metal mineralization (Fig. 4A and B). The Sb ± Au-Ag veins have N-S direction and are steeply dipping to W. These veins are hosted by andesite and are up to 400 m long, while the Sb mineralization reaches just 70–100 m to depth. Stibnite occurs on veins, lenses, and hydrothermal breccias in silicified and pyritized zones up to 5 m thick, but individual veins are just 0.1 m thick, rarely vein clusters are up to 0.7 m thick. The vein filling consists of quartz, carbonates (mostly dolomite), and chalcedony (in subsurface parts). Usually coarse-grained stibnite forms irregular, often monomineralic veins and nests in quartz, accompanied by later pyrite. Rarely, stibnite forms euhedral crystals up to 15 cm long. Rare baryte occurs in cavities with

quartz and chalcedony. At Nozger, cinnabar forms veinlets or occurs in cavities in quartz (Kaličiak and Ďuďa 1981; Ďuďa et al. 1981; Divinec et al. 1988; Ďuďa 1992).

Infrequently, stibnite also occurs in the base-metal veins in the central part of the ore field (in exploration drill holes and in the adits Gemerka, "3", and Mária). It is intergrown with quartz and carbonates, overprinted on the earlier base-metal and precious-metal mineral assemblages in veins and voluminous breccia zones (Fig. 4C). Locally in these veins, stibnite is associated with metastibnite and various Ag-Pb-Sb sulfosalts (Kovalenker et al. 1988; Ďuďa 1992), but this stibnite represents an earlier stibnite generation. According to Lexa et al. (2002), there are two generations of stibnite, the earlier being associated with Ag-Pb-Sb sulfosalts (Fig. 5). Most of the stibnite at this deposit belongs to the later stibnite generation, including the Sb ± Au-Ag veins.

Minor stibnite mineralization of stockwork-disseminated type is present south of the central zone at the Hg deposit Dubník and the precious-opal deposit Červenica (Fig. 4A). At Dubník, aggregates of small stibnite crystals are associated with pyrite, quartz, and marcasite in a NE-SW zone, spatially separated from the Hg mineralization. At Červenica, tiny stibnite crystals occur in cavities and fissures accompanied by hyalite, marcasite, and pyrite (Kaličiak and Ďuďa 1981).

In the N margin of the system, the Sb ± Au-Ag veins are accompanied by silicification, pyritization, and argillic alteration with smectite and minor kaolinite, while in S margin of the system wall-rock alteration is represented by illite/illite-smectite and minor kaolinite (Lexa et al. 2002).

Methods

For the combined Sb and S isotopic analyses fifteen stibnite samples from various parts of the two ore fields have been collected from historical mining collections archived at the Department of Mineralogy, Petrology and Economic Geology (Comenius University, Bratislava) and the Geological Institute of D. Štúr (in Bratislava and Košice). All samples with stibnite contained stibnite as the only ore mineral accompanied by quartz or chalcedony, probably representative of major stibnite crystallization events at both deposits. Additional samples for complementary sulfur isotope analyses included two stibnite and two pyrite samples from recent exploration drill holes in Kremnica, and five sphalerite samples from the Zlatá Baňa historical collections. Pure sulfide samples were fragmented from centimeter thick veins, sieved, hand-picked and all the samples were examined with a binocular microscope to confirm monomineral purity.

Stable sulfur isotopes were measured using an isotope ratio mass spectrometer (IRMS) MAT 253 coupled to an elemental analyzer Flash2000HT Plus via a continuous-flow interface ConFlo IV at the Slovak Academy of Sciences in Banská Bystrica (all Thermo Scientific). Separated samples of stibnite (150–400 µg) were powdered, mixed with about the same amount of V_2O_5, wrapped into tin capsules and combusted with oxygen in quartz tube filled with WO_3 and electrolytic copper at 1000 °C. Yielded SO_2 gas was purified on a packed GC-column (5 Å mol sieve at 90 °C) and introduced into the IRMS. Raw measurements were calibrated using two international reference materials IAEA-S2 and IAEA-S3 with + 22.70 and − 32.30‰ Canyon Diablo Troilite (CDT), respectively. Precision of measurements is 0.21‰, all the values are reported as per mil *versus* CDT. The obtained sulfur isotope data were complemented by an archived set of unpublished $\delta^{34}S_{CDT}$ data from both deposits, obtained in the years 1983 to 1986 at the D. Štúr Institute of Geology in Slovakia.

For Sb isotopic analyses, approximately 50 mg of each sample were dissolved in 15mL Teflon vials containing 4 mL of heated, ultra-pure aqua regia for more than 12 h. Complete dissolution of the samples was visually confirmed. Samples were diluted greater than 100,000 times in a 0.5 M nitric acid solution with trace HF (0.01 M) so that the Sn stays in solution. Samples did not require ion exchange chromatography as shown by previous studies (Lobo et al. 2012, 2014). We further checked this as reported in Zhai et al. (2021), where the processing of several samples with the chromatography yielded identical results for samples without chromatography.

The Sb isotopic compositions for all samples were measured on a Thermo Scientific Neptune Plus MC-ICP-MS at the Washington State University. As means to develop in house Sb standards (QA/QC verification of the results), we continued to analyze a stibnite sample that was reported in Zhai et al. (2021), samples 19xkss-2, and a HPS (high purity standard). Each sample was measured 3 times during the sessions and values fell within the reported value in Zhai et al. (2021). Solutions were measured in low resolution mode and in dry plasma and on peak background measurements were subtracted out of each measurement and the samples matched within 20% of the standard voltages. The background Sn and Sb isotope voltages were no greater than 3 millivolts on each mass and total procedural blanks did not exceed this measured background. Mass bias was corrected using an internal standard of Sn with the exponential law and values were then corrected using standard-sample-standard bracketing. The data are repeated 2 times and measured 30 ratios in each of these cycles. The standard deviation of the ratio measured is $\sim 2 \times 10^{-6}$, which is lower than the repeat analyses and that of the in-house stibnite and synthetic solution reported above.

Mass bias for Sb measurements was treated through doping with the NIST Sn isotope standard and using the exponential fractionation correction followed by

standard-sample-standard bracketing. Samples were diluted with a 70 ppb Sn (NIST 3136 A lot 140917) solution and standards for Sb (NIST 3102 A lot 140911 at 35 ppb) bracketed every two samples. Tin is an ideal element for mass bias correction as the ionization is similar to Sb and multiple studies have used Sn to correct for Sn mass bias. The data were corrected for mass bias with the use of $^{120}Sn/^{116}Sn$ and $^{124}Sn/^{116}Sn$ ratios of the NIST 3136 A Sn standard. Both results give nearly identical values for the corrected samples with the $^{124}Sn/^{116}Sn$ values at ±0.02‰, which is within the error of the measurements. Thus, the $^{124}Sn/^{116}Sn$ corrected values have been reported, and the corrected values with other Sn isotope values yield similar results. The analytical uncertainty for all samples is 0.02‰. The variations of the $^{123}Sb/^{121}Sb$ ratios are presented in delta notation based on the following expression:

$$\delta^{123}Sb = \left(\frac{(\delta^{123}Sb/\delta^{121}Sb)sample}{(\delta^{123}Sb/\delta^{121}Sb)s\,\mathrm{tan}\,dard} - 1 \right) \quad (1)$$

The δ values are multiplied by 1000 and reported in ‰. The errors of the analyses are calculated in the most conservative manner. Repeats have 2σ errors at 0.025‰, which is identical to the variation of the standard throughout the run.

Results

All samples used in this work were hand specimens with abundant stibnite hosted by quartz or chalcedony (Fig. 6). The stibnite crystals show their typical acicular morphology. Stibnite aggregates are either radial (Fig. 6A and D) or composed of individual, almost parallel crystals intergrown in the silica matrix (Fig. 6B and C). In the latter case, we interpret these textures as contemporaneous deposition of fine-grained silica and stibnite (or a precursor of stibnite).

The measured Sb and S isotopic composition is summarized in Table 1 and graphically shown in Fig. 7. The $\delta^{123}Sb$ values range from −0.15 to +1.28‰ in Kremnica and from +0.12 to +1.54‰ in Zlatá Baňa. The average value of +0.36‰ in Kremnica is somewhat lower than +0.49‰ in Zlatá Baňa, although the latter average is influenced particularly by the high $\delta^{123}Sb$ value for the sample ZB−5 (Table 1).

Corresponding sulfur isotope analyses ($\delta^{34}S$) of stibnite range from +0.04 to +2.34‰ in Kremnica and −3.88 to −2.11‰ in Zlatá Baňa. These data were complemented by sulfur isotope analyses that are not accompanied by Sb isotope data (in addition to the historical data). For Kremnica, they include two stibnite (+2.73 and +2.84‰ $\delta^{34}S$) and two pyrite sulfur isotope compositions (–0.56 and +0.82‰ $\delta^{34}S$). From Zlatá Baňa, six sphalerite samples provided the range from −1.42 to +0.55‰ $\delta^{34}S$.

Discussion

Models of behavior of antimony and sulfur isotopes

Both investigated isotopic systems show the same pattern of evolution in the $\delta^{123}Sb$ *versus* $\delta^{34}S$ space (Fig. 7). This pattern, at least for the $\delta^{123}Sb$ values, can be readily compared

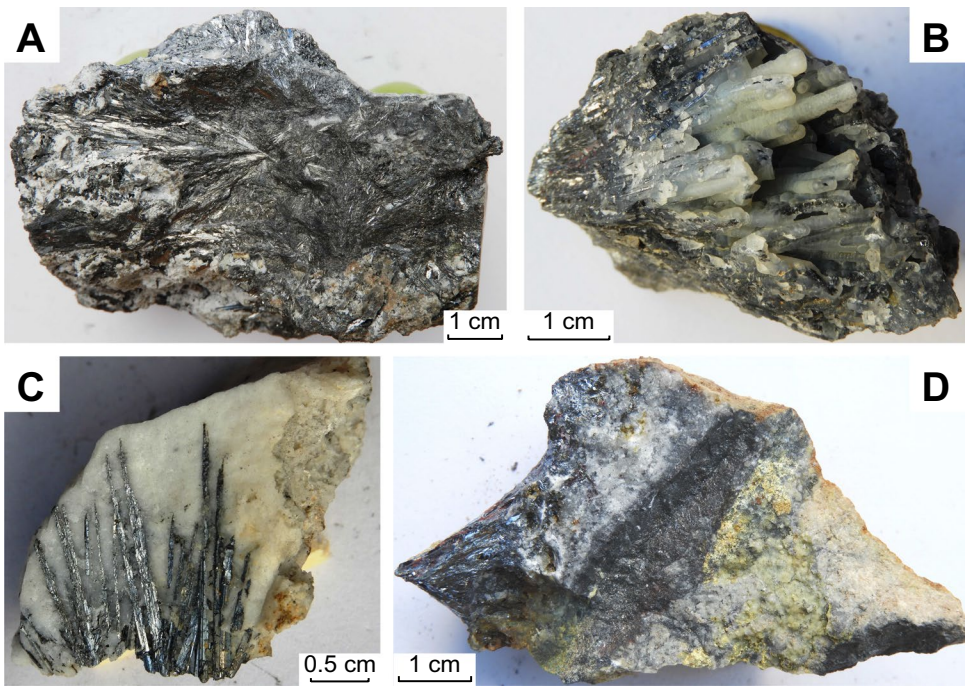

Fig. 6 Macrophotographs of representative hand specimens containing stibnite used in this research from the Kremnica (A = sample "Sb", B = 663/S) and Zlatá Baňa (C = ZB−3, D = ZB−4) deposits

Table 1 Measured $\delta^{123}Sb$ and $\delta^{34}S$ values of stibnite and complementary $\delta^{34}S$ values of other sulfides from Kremnica and Zlatá Baňa

Sample ID	Location	Mineral	$\delta^{34}S$	$\delta^{123}Sb$
Kremnica				
A1	Ferdinand adit, Krížna vein, IV. level, 2nd vein system	stibnite	+2.01	+0.63
A2	Ferdinand adit, 2nd vein system	stibnite	+0.50	+1.28
A4	Ferdinand adit, Krížna vein II. 12 m, 2nd vein system	stibnite	+2.34	+0.87
A3	Helena vein, 2nd vein system	stibnite	+1.76	+0.34
382/ 75	Šturec, 1st vein system	stibnite	+0.89	+0.43
A5	Šturec – Václav adit, 1st vein system	stibnite	+1.27	−0.15
Sb	Šturec, 1st vein system (Fig. 4a)	stibnite	+1.62	+0.09
383 / 74	Šturec, 1st vein system	stibnite	+1.17	−0.04
663 / S	Šturec – Václav adit (Fig. 4b)	stibnite	+1.26	+0.01
380/ 75	Šturec, 1st vein system	stibnite	+0.04	+0.10
UGA30-105.3	drill hole UGA30, Andrej adit, Šturec, 1st vein system	stibnite	+2.73	
UGA03-168.4	drill hole UGA03, Andrej adit, Šturec, 1st vein system	stibnite	+2.84	
UGA32-20.3	drill hole UGA32, Andrej adit, Šturec, 1st vein system	pyrite	+0.82	
UGA38-27.6	drill hole UGA38, Andrej adit, Šturec, 1st vein system	pyrite	–0.56	
Zlatá Baňa				
ZB-2	adit „3“, SL−1/127.0 m	stibnite	−2.93	+0.21
ZB-3	adit „3“, SL−1/131.2 m (Fig. 4c)	stibnite	−2.77	+0.27
ZB-5	adit „3“, SL−1/135.4 m	stibnite	−3.94	+1.54
ZB 1 J	adit Gemerka, SL−4, 15.5 m	stibnite	−2.11	+0.35
ZB-4	Gašpar vein, sample from heap of the adit (Fig. 4d)	stibnite	−3.28	+0.12
ZBS1	adit Gemerka, Sm−3/16.5 m	sphalerite	+0.55	
ZBS2	adit Gemerka, P−5/34.0 m	sphalerite	−0.94	
ZBS3	adit „3“, SL−1/84.0 m	sphalerite	−1.16	
ZBS4	adit Gemerka, SL−6/42.3 m	sphalerite	−0.75	
ZBS5	drill hole ZBT−4B/11 129.1 m, central part	sphalerite	−1.42	

to the recent studies of Zhai et al. (2021) and Kaufmann et al. (2023). These authors determined that within one mineralization stage, the $\delta^{123}Sb$ values in an ore-forming system evolve in a monotonous fashion, increasing as the precipitation of Sb minerals proceeds. Zhai et al. (2021) used this trend in the $\delta^{123}Sb$ values to determine the direction of fluid flow. Kaufmann et al. (2023) found that this trend applies not only to stibnite as the dominant Sb mineral, but also to other Sb minerals, such as gudmundite, berthierite, antimony, senarmontite, and kermesite. The limited data sets available suggest that such isotopic trends could be common, and we assume that they also apply in the case of the epithermal systems studied here.

Zhai et al. (2021) roughly estimated the Sb isotope fractionation factor between stibnite and fluid as $\alpha_{fluid-stibnite} = 0.9994$. No relation of this datum to temperature or Sb speciation in the fluid is known. The analysis of the data in Kaufmann et al. (2023), however, showed that this $\alpha_{fluid-stibnite}$ value could be used as a rough proxy to explain the existing observations in natural assemblages of primary minerals. Kaufmann et al. (2023) applied a simple Rayleigh fractionation model with the $\alpha_{fluid-stibnite}$ value 0.9994 to show that all measured $\delta^{123}Sb$ values can be reproduced.

Assuming that the gradual increase of the $\delta^{123}Sb$ values corresponds to the precipitation progress in a hydrothermal system, a correlation with $\delta^{34}S$ values can be discerned (Fig. 7). We emphasize again that the evolution of the $\delta^{123}Sb$ values was inferred based on the previous studies. In the studied material, stibnite aggregates are dispersed in a quartz-chalcedony gangue and the relative temporal position of the individual stibnite samples with respect to each other cannot be determined. We assume that initially, the $\delta^{34}S$ values increase by about 2‰ but they drop for the latest stibnite precipitate. The trend is similar for both investigated deposits even though the $\delta^{34}S$ values in Kremnica are systematically higher than those in Zlatá Baňa.

The variations in both $\delta^{123}Sb$ and $\delta^{34}S$ values suggest that the S pool in the fluid was not significantly larger than the Sb pool. If there was much more S than Sb, the fraction of removed S by stibnite precipitation would be too small to cause such significant changes in the $\delta^{34}S$ values. An alternative explanation is that the

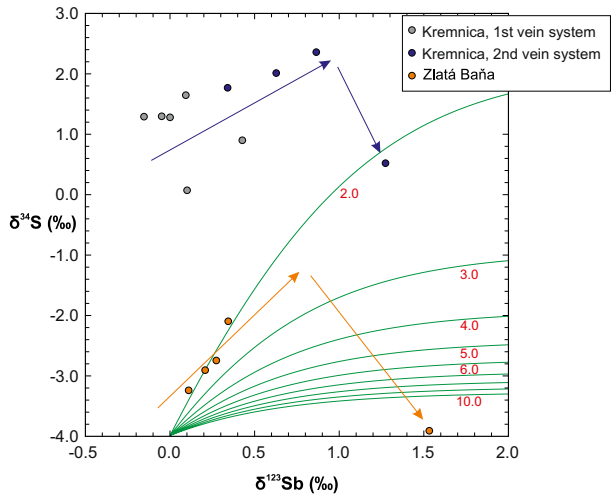

Fig. 7 Isotopic composition of stibnite samples from Zlatá Baňa (orange), Kremnica 1st vein system (gray), and Kremnica 2nd vein system (blue). The blue and orange arrows show the assumed evolution of the Sb-S isotopic values. The green curves show the simultaneous Rayleigh fractionation of Sb and S isotopes upon stibnite precipitation according to the Eqs. (3) and (4). They show the isotopic composition of the instantaneous product, i.e., stibnite. The curves are labeled by the molar ratios m_S/m_{Sb} in the fluid (small red numbers). The starting fluid for the samples from Zlatá Baňa has the composition 0.6‰ δ^{123}Sb and 0.4‰ δ^{34}S, and the $\alpha_{stibnite-H2S}$ factor was calculated for 150 °C. The very first stibnite crystal has composition of 0.0‰ δ^{123}Sb and −4.0‰ δ^{34}S. Note that the starting composition can be arbitrarily chosen, resulting simply in the translation of the calculated (green) curves. For the Kremnica samples, the starting point should be chosen with a higher δ^{34}S than for the Zlatá Baňa samples

S pool in the form of H_2S(aq) and HS^- species was isotopically decoupled from the Sb(III) species, especially $H_2Sb_2S_4$(aq) or its deprotonated forms (Bessinger and Apps 2005). The studied ores, however, are dominated by quartz, with small amounts of sulfides, suggesting that the concentration of sulfur in the fluids was not high. This hypothesis would favor the former possibility above. Namely, these fluids carried small amount of Sb species but also a small amount of S species other than the Sb-S aqueous species.

For the precipitation of stibnite from a hydrothermal fluid and associated isotopic changes, a Rayleigh model can be constructed. In such a model, the isotopic composition of the instantaneous product is

$$\delta = f^{\epsilon}(\delta_0 + 1) - 1 + \epsilon \tag{2}$$

where δ is the isotopic composition of the instantaneous product, δ_0 is the initial isotopic composition of the system, f is the fraction of the reactant removed from the system, and $\varepsilon = \alpha - 1$. It is assumed that the instantaneous product is removed from the system and does not interact with the remaining fluid or the previously formed product. For the systems investigated here,

$$\delta^{123}Sb = f_{Sb^{\epsilon}\_Sb}(\delta^{123}Sb_0 + 1) - 1 + \epsilon_{Sb} \tag{3}$$

$$\delta^{34}S = f_{S^{\epsilon}\_S}\ (\delta^{34}Sb_0 + 1) - 1 + \epsilon_S \tag{4}$$

For this model, we assume Sb isotope fractionation factor $\alpha_{fluid-stibnite} = 0.9994$ (Zhai et al. 2021). The magnitude of S isotope fractionation between stibnite and H_2S is $\Delta_{stibnite-H2S} = -3.4$ (at 200 °C) or −5.4‰ (at 100 °C; Ohmoto and Rye 1979), translating to $\alpha_{stibnite-H2S} = 0.9966$ (at 200 °C) or $\alpha_{stibnite-H2S} = 0.9946$ (at 100 °C).

In our case, it is assumed that stibnite is the only precipitating solid that harvests Sb and S from the fluid; no other sulfide or Sb phase precipitates. This assumption couples the Eqs. (3) and (4) because the fraction of removed Sb and that of removed S is given by the initial amount of Sb and S in the fluid and by the stoichiometry of stibnite (Sb_2S_3). In general, the ratio of the fractions removed is

$$\frac{\triangle f_{Sb}}{\triangle f_S} = \frac{2m_{Sb_2S_3}/m_{Sb}}{3m_{Sb_2S_3}/m_S} \tag{5}$$

where m_Sb_2S_3 is the number of moles of stibnite precipitated, m_{Sb} is the total Sb molality in the fluid, and m_S is the total S molality in the fluid. For convenience, consider that 1 mol of stibnite precipitates. The Eq. (5) reduces to

$$\frac{\triangle f_{Sb}}{\triangle f_S} = \frac{2/m_{Sb}}{3/m_S} = \frac{2}{3} \times \frac{m_S}{m_{Sb}} \tag{6}$$

It is also assumed that Sb is found in the $(H_xSb_2S_4)^{2-x}$ species, for example in $HSb_2S_4^-$, and reduced sulfur either as HS^- or H_2S^0. Under this assumption

$$m_{Sb} = 2m(HSb2S_4^-) \tag{7}$$

and

$$m_S = 4m(HSb_2S_4^-) + m(HS^-) + m(H_2S^0) \tag{8}$$

An extreme scenario would be represented by a fluid where both Sb and S occur exclusively in the $HSb_2S_4^-$ species and any other aqueous species are effectively removed from the fluid. Precipitation of stibnite would proceed according to the reaction

$$HSb_2S_4^- = Sb_2S_3 + HS^- \tag{9}$$

Below, we present two examples as model cases of behavior of antimony and sulfur isotopes at contrasting Sb/S ratio in the fluid:

The first example includes a fluid with the initial molality ratio m_S/m_{Sb} near to 2.0. In such a fluid, antimony and sulfur

occur mostly in the $HSb_2S_4^-$ species with a small amount of other S species. The ratio of fraction of removed Sb to the fraction of removed S (Δf_{Sb} / Δf_S) is 1.333. Under the assumption that HS^- is continuously removed from the fluid, the molality ratio m_S/m_{Sb} remains nearly constant.

In the second example, consider a fluid with initial $m_S/m_{Sb} = 10$, i.e., with tenfold more sulfur than antimony. Thus, a significant proportion of other S species than $HSb_2S_4^-$ are present in such a fluid. The ratio of the fractions removed Δf_{Sb} / Δf_S is 6.667. This value means that if precipitation of a certain amount of antimony removes 0.1% of sulfur from the fluid ($\Delta f_S = 0.001$), then this action removes 0.6667% of Sb from the fluid ($\Delta f_{Sb} = 0.006667$). This model is graphically shown by green curves in the Fig. 7. The slope of the data points for the samples from Zlatá Baňa can be well described with a fluid with m_S/m_{Sb} ~ 2. On the other hand, the data from Kremnica are better described by a fluid with more sulfur, with m_S/m_{Sb} ~ 3–4. These two coupled Rayleigh models reproduce the rise of the $\delta^{34}S$ values of stibnite that is concomitant with the gradual increase in the $\delta^{123}Sb$ values. The numerical values of the m_S/m_{Sb} from both localities are similar and show that the fluids did not possess a significant excess of sulfur with respect to antimony.

The sudden drop of the $\delta^{34}S$ values at the end of stibnite precipitation must be explained by a different process. Mineralogical and textural evidence suggests that the late stages of stibnite precipitation were accompanied by pyrite/marcasite and baryte (at Zlatá Baňa). The fractionation magnitude of the sulfides is $\Delta_{pyrite-H2S} = +1.8$ (at 200 °C) or +2.9‰ (extrapolated to 100 °C; Ohmoto and Rye 1979). These values show that precipitation of pyrite or marcasite depletes the fluid in the heavier isotope (^{34}S) and results in the drop of the $\delta^{34}S$ values of the subsequently precipitated sulfide minerals. A similar effect with much larger fractionation is associated with the oxidation of sulfide to sulfate, with $\Delta_{sulfate-H2S}$ of +29.5 (at 200 °C) or +43.8‰ (extrapolated to 100 °C; Ohmoto and Rye 1979). It follows that a substantial precipitation of pyrite/marcasite or even a minor precipitation of baryte would have caused depletion of the heavy sulfur isotopes in the fluid, resulting in a progressively lighter composition of subsequently formed pyrite/marcasite and stibnite. This is consistent with the fact that the historical and recent $\delta^{34}S$ values of pyrite/marcasite samples are quite variable, ranging from −12.4 to +5.0‰ $\delta^{34}S$ (median +2.0‰) in Kremnica and from −3.0 to +1.5‰ $\delta^{34}S$ (median −1.3‰) in Zlatá Baňa (Fig. 8). Furthermore, this is also in agreement with highly positive historical sulfur isotopic composition of sulfates from the north of the Kremnica vein system (gypsum + 17.0‰ and anhydrite + 23.9‰ $\delta^{34}S$) and from Zlatá Baňa (baryte + 22.1‰ $\delta^{34}S$) (Štohl et al. 1994). However, the temporal link of sulfates to the stibnite mineralisition is not clear, as sulfates/anhydrite in Kremnica can be related to weathering (Böhmer 1966) and baryte in Zlatá Baňa precipitated during two different stages (Ďuďa 1992; Chovan et al. 1994).

Difference in sulfur isotope composition at both deposits

There is a difference between stibnite $\delta^{34}S$ values from the two studied deposits, as Kremnica stibnite is about 4.4‰ heavier than the stibnite from Zlatá Baňa. Interestingly, a

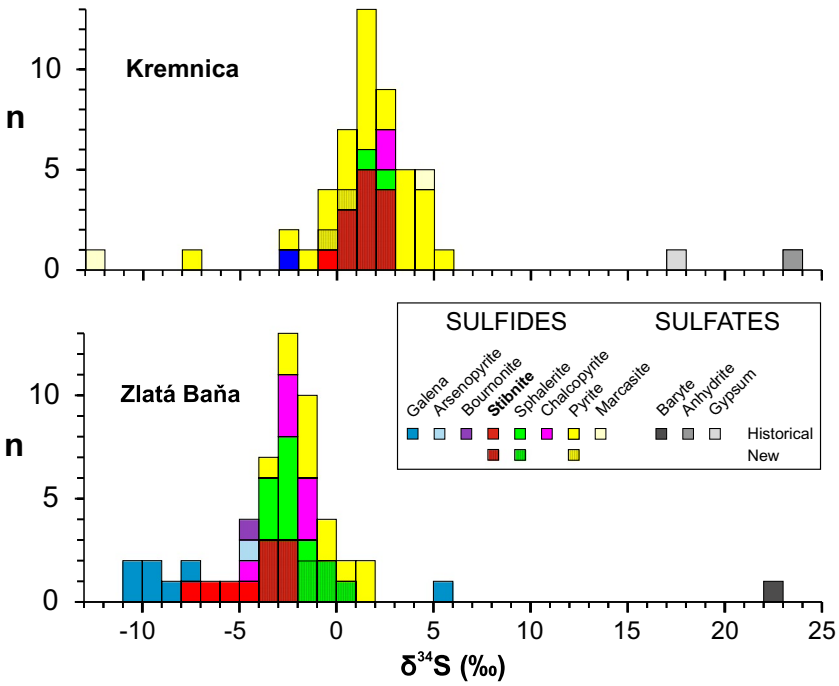

Fig. 8 Comparison of the sulfur isotopic composition ($\delta^{34}S$) of various sulfides and sulfates from the Kremnica and Zlatá Baňa deposits. Most of the data come from earlier studies published in Štohl et al. (1994) and archived at the D. Štúr Institute of Geology in Bratislava, Slovakia, but they also include new analyses from this work

similar $\delta^{34}S$ difference is also observed in other sulfides from the two deposits, including the sulfides from earlier, higher-temperature stages (Fig. 8). In Kremnica, nearly all sulfides (pyrite, sphalerite, galena, chalcopyrite, marcasite) show $\delta^{34}S$ values between −2.3 and +5.0‰, (excluding two outliers), while in Zlatá Baňa various base-metal minerals show mostly negative values ($\delta^{34}S$ of −10.3 to +1.5‰, excluding one outlier). Thus, the difference in stibnite $\delta^{34}S$ values is probably related to the different isotopic composition of the parental hydrothermal fluids and not to specific conditions of stibnite precipitation at either of the studied deposits. Since the isotopic composition of sulfides from Kremnica veins are similar to those from epithermal veins in the neighboring Štiavnica stratovolcano (Štohl et al. 1994; Maťo et al. 1996), sharing the same volcanic field, we assume that the systematic difference in sulfur isotopic composition could be related to the different magmatic-hydrothermal evolution of the Central and Eastern Slovak Volcanic Fields.

Most magmas that are feeding porphyry and epithermal systems have their total S isotope values between 0 and +5‰ (Hutchison et al. 2020). There could be several reasons for variation in isotopic composition of calc-alkaline hydrothermal systems such as crustal assimilation, degassing processes, and a slab-influenced mantle source (McKibben et al. 1996; De Hoog et al. 2001; Field et al. 2005). Furthermore, S isotope fractionation that occurs due to magmatic degassing and sulfide segregation is strongly dependent on redox conditions and diminishes ^{34}S concentration in the residual melt (Hutchison et al. 2019).

It is not clear, however, what caused the different composition of magmatic sulfur from both volcanic fields studied here. Such distinction is, however, beyond the scope of this study and does not affect the interpretations presented above. We only note that the Central Slovak Volcanic Field (host of the Kremnica deposit) contains much more and larger ore deposits than the Eastern one (host of the Zlatá Baňa deposit), thus future research on this observation could aid in better understanding of the regional metallogeny and lithospheric processes related to Neogene volcanism in the Western Carpathians.

Interpretation of Sb transport and stibnite precipitation

In hydrothermal fluids, the mobility of Sb depends on the temperature, pH, and sulfur fugacity. Experimental studies and thermodynamic modeling at various physicochemical conditions suggest that Sb is transported in hydrothermal fluids as Sb(III) in $HSb_2S_4^-$, $Sb_2S_4^{2-}$, $Sb(OH)_3$, $Sb(OH)_2Cl$ and $SbCl^{2+}$ complexes (Zotov et al. 2003; Pokrovski et al. 2006; Obolensky et al. 2007; Olsen et al. 2018, 2019). According to the thermodynamic models of Obolensky et al. (2007) for temperatures 200–250 °C, the highest Sb-transporting capacity have hydrothermal fluids that are poor in reduced sulfur species and are either acidic (pH = 2–3) with high chlorinity or alkaline (pH = 7–8) with low-chlorinity.

In hydrothermal Sb deposits, stibnite is often abundant in late mineralization stages and generally precipitates from moderately saline fluids (3.5–6.5 wt% NaCl equiv.) at low temperature (< 200 °C) (Wiliams-Jones and Normand 1997; Bailly et al. 2000). According to Koděra et al. (2014), the mineralizing fluids in Kremnica were of low salinity (< 2 wt% NaCl eq.) and predominantly of meteoric origin. These fluids experienced extensive boiling and gradual decrease in temperature along the system (~ 270–140 °C) related to a N-S trending decrease in erosion level from ~ 500 to 50 m (Koděra et al. 2014). Cryptocrystalline quartz from the veins with stibnite at Šturec has the highest $\delta^{18}O$ values of vein quartz (+13.8 to +18.8‰) in the entire ore field, interpreted to originate above the boiling level of paleofluids at temperatures ~ 90–130 °C based on the oxygen isotope geothermometry. Furthermore, fluid inclusions microthermometry data from dolomite from the earlier quartz-carbonate sub-stage (5) of the Sb ± Hg, As stage provided homogenization temperatures in the range 120–181 °C and similar values were also obtained from the oxygen isotope geothermometry of carbonates (Koděra et al. 2014). In Zlatá Baňa, the base-metal mineralization formed at 300–200 °C, while the Au-Ag mineralization formed below 200 °C (Štohl et al. 1994). According to Jeleň and Kovalenker (1995), the Sb ± Au-Ag mineralization crystallized here from fluids at 200–150 °C.

As presented above, the stibnite mineralization at Kremnica and Zlatá Baňa deposits crystallized from a low-salinity fluid at temperature much below 200 °C. The low salinity is typical for low-sulfidation epithermal systems as their fluids have a significant proportion of meteoric water (e.g., Cooke and Simmons 2000; Sillitoe and Hedenquist 2003; Simmons et al. 2005), while the lower crystallization temperature is likely caused by a low total Sb concentration in the fluid. This results from the decreasing solubility of Sb with decreasing temperature, meaning that the fluids low in Sb can reach the supersaturation initially at the lower temperatures. According to the modeling results of this study on the behavior of Sb and S isotopes, the speciation of Sb in these fluids was dominated by the $HSb_2S_4^-$ species with a variable amount of other S species.

Temperature decrease is considered as the main mechanism of stibnite precipitation, especially if Sb is mainly transported as a neutral hydroxy species (Williams-Jones and Normand 1997; Zotov et al. 2003). For instance, stibnite crystallization at the Hishikari Au-Ag deposit has been attributed to the quick cooling of the hydrothermal system from ~ 200 °C down to ~ 110 °C, based on fluid inclusion data in quartz and stibnite, respectively (Ueno et al. 2001; Shimizu 2018). However, a sharp decrease in pH could be also a principal cause of stibnite mineralization (Williams-Jones and Normand 1997; Simpson

et al. 2015), as suggested by the thermodynamic models of Obolensky et al. (2007). The combined effects of decreasing pH and aH_2S on stibnite solubility are illustrated by the reaction in the predominance field of H_2S(aq), approximately below pH = 7 at 125 °C.

$$HSb_2S_4^- + H^+ = Sb_2S_3 + H_2S \quad (10)$$

The consumption of H^+ in the fluid could result in an increase in pH, while the excess of H_2S could be subsequently used for the precipitation of late sulfidic minerals, such as pyrite/marcasite, as observed at both studied deposits (Figs. 3 and 5). The expected pH changes of the fluids are suggested by the common presence of kaolinite, originating from fluids with lower pH. This kaolinite is accompanied by clay minerals linked to higher pH fluids and even carbonates (in Kremnica).

The experimental data on stibnite solubility are supported by data from active geothermal fields in volcanic areas with a high geothermal gradient, which are generally recognized as modern analogues of epithermal systems. Wilson et al. (2007) have shown that both a pH change (acidification) and a temperature decrease are the principal causes of stibnite deposition in geothermal wells of two power stations in New Zealand. At Rotokawa, an acidic condensate injected into a well is probably responsible for the stibnite precipitation, rather than the overall drop in temperature from 224 to 151 °C. At Ngawha, temperature dropped to < 100 °C and over the same time period, an order of magnitude more stibnite was formed in heat exchangers in Ngawha than in Rotokawa. These observations confirm that the temperature change is a more efficient mechanism for stibnite precipitation in the geothermal wells. Furthermore, antimony was not detected in vapor-line samples. That is in agreement with the assumption that Sb complexes are mostly transported through aqueous fluids.

At Kremnica and Zlatá Baňa, both mechanisms could have contributed to stibnite crystallization (Fig. 9). As stibnite precipitation occurred in final stages of hydrothermal activity, cooling of fluids was certainly an important factor. The acidification of the fluids, however, could be also of importance if considering that the transport of Sb was facilitated predominantly by the $HSb_2S_4^-$ species. The acidification of fluids is documented by the presence of illite-kaolinite ± smectite halos around the quartz veins, whereas kaolinite (as the product of acidic alteration) especially occurs in upper parts of both deposits (Böhmer 1966; Bačo in Lexa et al. 2002). The clay minerals in the halos are accompanied by pyrite and carbonates. According to Hedenquist and Arribas (2022), such mineral assemblage indicates the involvement of a steam-heated CO_2-rich condensate that is commonly present on the margins and at the end of the lifetime of epithermal systems. These solutions are related to CO_2- and H_2S-bearing vapors that originate from parental boiling liquid in the deep upflow. The gaseous components condense into meteoric water below the water table and react to carbonic-acid solutions with pH of 4–5:

$$CO_2 + H_2O \leftrightarrow H_2CO_3 \leftrightarrow HCO_3^- + H^+ \quad (11)$$

The condensate typically forms a solution at several hundreds of meters depth, with temperatures of ~ 120–170 °C

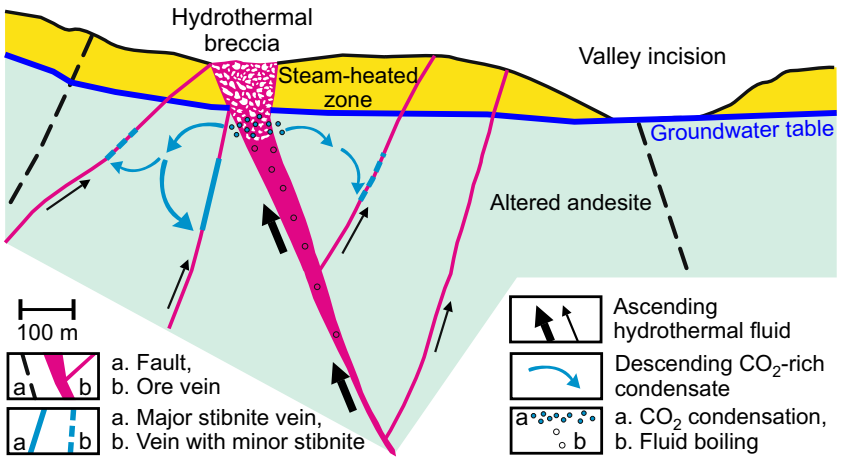

Fig. 9 Schematic model for the origin of stibnite-bearing veins in late stages and on margins of the low- to intermediate-sulfidation systems. Efficient precipitation of stibnite is related to cooling of ascending hydrothermal fluids, further enhanced by mixing with a mildly acidic CO_2-rich condensate. The transport of Sb is predominantly in $HSb_2S_4^-$ species which are sensitive to cooling and acidification. Condensation of CO_2- and H_2S-bearing vapors is related to the boiling of hydrothermal fluid in deep upflow zones in the major fluid conduits. The gaseous components condense into a heated meteoric water below the water table, with only a minor sulfate formation. In contrast, the steam-heated zone above the water table is affected by acidic leaching due to the oxidation of H_2S. The model was created using the schemes in Sillitoe (2015) and Hedenquist and Arribas (2022)

and devoid of electrolytes. It subsequently acts as a diluent of the ascending, electrolyte-richer liquids. Sulfate formation in the condensate is minor because of the low dissolved oxygen content in meteoric water below the water table (Reyes 1990; Simpson et al. 2001; Simmons et al. 2005; Hedenquist and Arribas 2022). Thus, the sufficiently cooled and near-neutral late-stage Sb-bearing fluids could probably interact and mix with the steam-heated, mildly acidic, CO_2-rich condensate (Fig. 9). The combination of the processes made the precipitation of stibnite more efficient than just simple fluid cooling, even if the fluid contained just sub-ppm concentrations of Sb (Simpson et al. 2015). This interpretation is also supported by the location of the stibnite-bearing veins mostly on the margins of both studied epithermal deposits where the presence of the CO_2-rich condensates is most common in low- and intermediate sulfidation epithermal systems (Hedenquist and Arribas 2022).

The data available make the distinction between fractionation in an open or in a closed system only partially possible. Natural systems can be subject to fluid influx (magmatic fluid input, mixing with meteoric water, mixing with condensate) or fluid loss (e.g., by boiling). They can also behave almost as a closed system, as proposed recently by another Sb isotope study on stibnite (Zhai et al. 2021). Continuous or pulsed input of magmatic fluids would likely lead to resetting of the isotopic signature of both Sb and S that is not observed. A continuous flow of magmatic fluids would be able to explain the observed isotopic trends if it is assumed that isotopic fractionation occurs in the fluid source, i.e., in the magma reservoir. Our work at the two deposits and works at additional deposits elsewhere (Zhai et al. 2021; Kaufmann et al. 2023) suggest that these isotopic changes are generated in the fluid reservoir in the hydrothermal veins, not in the source of the metals and sulfur. Boiling of the epithermal fluid should lead to a monotonous shift towards lighter (in the gaseous phase) or heavier (in the liquid phase) isotopes. Initially, both $\delta^{34}S$ and $\delta^{123}Sb$ move indeed towards higher values (Fig. 7) and a contribution from boiling cannot be excluded. The model presented here, however, does not require additional fractionation from boiling; the fractionation factors for mineral precipitation suffice to explain the isotopic trends. The sudden drop of $\delta^{34}S$ values is most easily explained by precipitation of late pyrite, marcasite, or sulfates as discussed above. Dilution with meteoric water would lead to cooling and stibnite precipitation. Similarly, dilution with a steam-heated condensate fluid, typical for near-surface portions of epithermal systems, would trigger stibnite precipitation by acidification of the fluids. Unless the meteoric fluid or the condensate would have brought significant Sb and S amounts into the system, such fluid mixing would be very difficult to identify from the data in the deposits studied here. The evidence gathered in this work speaks against a significant input of magmatic fluid influx or fluid loss *via* boiling. Fluid mixing with meteoric and/or condensate fluids is documented by other lines of evidence outlined above, even though it cannot be identified from the isotopic data alone. Hence, the system was probably open with respect to fluid mixing where the external fluids (meteoric, condensate) did not contribute much to the Sb and S budget. These fluids only triggered and sustained stibnite precipitation.

Conclusions

Antimony ($\delta^{123}Sb$) and sulfur ($\delta^{34}S$) isotope composition of stibnite in the Kremnica and Zlatá Baňa deposits helped to better understand the transport and precipitation of this mineral in low- to intermediate-sulfidation epithermal systems. The observed increase in the $\delta^{123}Sb$ values of stibnite concomitant with the gradual increase in $\delta^{34}S$ values corresponds to the progressive precipitation of stibnite and suggest that the S pool in the parental fluid was not significantly larger than the Sb pool. The process can be well reproduced by two coupled Rayleigh fractionation models, assuming that the fluids transported Sb species predominantly in the form of $HSb_2S_4^-$ with a small and variable amount of other S species. According to the models, samples from Zlatá Baňa are related to a fluid with molar ratios $m_S/m_{Sb} \sim 2$, while the samples from Kremnica correspond to a fluid with $m_S/m_{Sb} \sim 3–4$. The sudden decrease in the $\delta^{34}S$ values at the heaviest $\delta^{123}Sb$ values of stibnite can be explained by a substantial precipitation of pyrite/marcasite or a minor precipitation of baryte at the end of stibnite precipitation.

The parental fluids of stibnite-bearing veins were of low-salinity (< 2 wt% NaCl eq.) and of low temperature (< 150 °C). Temperature decrease is considered as the main mechanism of stibnite precipitation, along with acidification of the Sb-bearing hydrothermal fluid. These findings agree with observations from active geothermal fields. Acidification is likely related to mixing with a mildly acidic fluid of a steam-heated CO_2-rich condensate that is commonly present on margins and at the end of the lifetime of epithermal systems. This explains the location and timing of stibnite-bearing veins predominantly on the margins of both studied epithermal deposits.

Acknowledgements Two anonymous reviewers are thanked for their helpful reviews. Mike Gadd is acknowledged for editorial handling. This study was supported by the grant of the Research Agency of the Ministry of Education, Science, Research and Sport of the Slovak Republic (contract No. VEGA 1/0313/20) and by the grant of the Slovak Research and Development Agency (contract No. APVV-22-0134). Peter Čech is acknowledged for providing records of sulfur isotope data from Kremnica and Zlatá Baňa, archived at the D. Štúr Institute of Geology in Bratislava, Slovakia. Matej Rybárik and Peter Toth are acknowledged for their help in separation of minerals for isotope analyses. J.Majzlan was financially supported by a Deutsche Forschungsgemeinschaft grant MA 3927/43 – 1. R. Mathur acknowledges NSF EAR grant no. 2233426.

Author contributions The first draft of the manuscript was written by Peter Koděra and Juraj Majzlan, and all authors commented on subsequent versions of the manuscript. Juraj Majzlan was especially responsible for calculations of Rayleigh fractionation models. Isotopic analyses were performed and organized by Ryan Mathur and Degao Zhai (Sb isotopes) and Rastislav Milovský (S isotopes). Pavol Bačo was involved in sampling of all sulfides from Zlatá Baňa and provided geological and mineralogical background for these samples. All authors read and approved the final version of the manuscript.

Funding Open access funding provided by The Ministry of Education, Science, Research and Sport of the Slovak Republic in cooperation with Centre for Scientific and Technical Information of the Slovak Republic. This study was supported by the grant of the Research Agency of the Ministry of Education, Science, Research and Sport of the Slovak Republic (contract No. VEGA 1/0313/20) and by the grant of the Slovak Research and Development Agency (contract No. APVV-22-0134). Juraj Majzlan was financially supported by a Deutsche Forschungsgemeinschaft grant MA 3927/43 – 1. Ryan Mathur acknowledges NSF EAR grant no. 2233426.

Declarations

Competing interests The authors have no competing interests to declare that are relevant to the content of this article.

References

Bailly L, Bouchot V, Beny C, Milesi J (2000) Fluid inclusion study of stibnite using infrared microscopy: an example from the Brouzils antimony deposit (Vendee, Armoriscan Massif, France). Econ Geol 95:221–226

Bakos F, Chovan M, Bačo P, Bahna B, Ferenc Š, Hvožďara P, Jeleň S, Kamhalová M, Kaňa R, Knésl J, Krasnec Ľ, Križáni I, Maťo Ľ, Mikuš T, Pauditš P, Sombathy L, Šály J (2004) Gold in Slovakia. Slovenský skauting, Bratislava. (in Slovak with English summary)

Bartalský B, Finka O (1999) New results of the geological exploration of the 1st vein system of the Kremnica precious metal veins. Mineralia Slovaca 31:291–296 (in Slovak)

Bessinger B, Apps JA (2005) The hydrothermal chemistry of gold, arsenic, antimony, mercury and silver. Report LBNL-57395

Böhmer M (1966) Geology and mineral associations of gold-bearing veins in the central part of the Kremnica ore field. Acta Geol Geogr Univ Comenianea Geologica 11:5–123 (in Slovak)

Böhmer M (1977) Deep structures of the Kremnica ore field. Open file report, Archive of the State Geol Institute of D. Štúr, Bratislava (in Slovak)

Böhmer M (1980) Stibnite on subvolcanic veins of the Kremnické ore field. Proceedings of the conference Antimony ore mineralizations of Czechoslovakia, pp 157–164 (in Slovak)

Böhmer M, Škvarka L (1970) The relationship between footwall of Neogene volcanic rocks and effluences of thermal water in Kremnica. Geologické práce, správy 53: 21–32 (in Slovak)

Böhmer M, Gerthofferová H, Kraus I (1969) To the problems of alterations of central Slovakia Neovolcanites. Geologický Zborník Geol Carpath 20:47–68

Chovan M, Háber M, Jeleň S, Rojkovič I (1994) Ore textures in the Western Carpathians. Slovak Academic Press, pp 1–219

Cooke DR, Simmons SF (2000) Characteristics and genesis of epithermal gold deposits. In: Hagemann G, Brown PE (eds) Gold in 2000. Rev Econ Geol 13:221–244

Corbett GJ, Leach TM (1998) Southwest Pacific gold-copper systems: structure, alteration and mineralization. Soc Econ Geol Spec Publ 6

De Hoog JCM, Taylor BE, Van Bergen MJ (2001) Sulfur isotope systematics of basaltic lavas from Indonesia: implications for the sulfur cycle in subduction zones. Earth Planet Sci Lett 189:237–252

Divinec Ľ, Kotuľák R, Repčiak M, Kaličiaková E, Duďa R (1988) Zlatá Baňa deposit in the light of new geological survey data. Mineralia Slovaca 20:221–238 (in Slovak)

Ďuďa R (1992) Mineralogical-paragenetical relationships in the Zlatá Baňa ore field (Slánske vrchy Mts). PhD Thesis, Technical University Košice (in Slovak)

Ďuďa R, Černý P, Kaličiak M, Tözsér J, Ulrych J, Veselovský F (1981) Mineralogy of the north part of the Slanské vrchy Mts. Mineralia Slovaca Monograph 2, Alfa, Bratislava (in Slovak)

Field CW, Zhang L, Dilles JH, Rye RO, Reed MH (2005) Sulfur and oxygen isotopic record in sulfate and sulfide minerals of early, deep, pre-Main stage porphyry Cu-Mo and late Main Stage base-metal mineral deposits, Butte district, Montana. Chem Geol 215:61–93

Finka O (2009) Wealth hidden in earth, history and present of the gold deposit in Kremnica. Krupa print, s.r.o., Žilina (in Slovak with English summary)

Hagemann SG, Lüders V (2003) P-T-X conditions of hydrothermal fluids and precipitation mechanism of stibnite-gold mineralization at the Wiluna lode-gold deposits. Western Australia: conventional and infrared microthermometric constraints. Min Depos 38:936–952

Hedenquist JW, Arribas A (2022) Exploration implications of multiple formation environments of advanced argillic minerals. Econ Geol 117:609–643

Hedenquist JW, Arribas A, Gonzalez-Urien E (2000) Exploration for epithermal gold deposits In: Hagemann SG, Brown PE (eds) Gold in 2000. Rev Econ Geol 13:245–277

Hutchison W, Babiel RJ, Finch AA, Marks MAW, Markl G, Boyce AJ, Stüeken EE, Friis H, Borst AM, Horsburgh NJ (2019) Sulphur isotopes of alkaline magmas unlock long-term records of crustal recycling on Earth. Nat Commun 10

Hutchison W, Finch AA, Boyce AJ (2020) The sulfur isotope evolution of magmatic-hydrothermal fluids: insights into ore-forming processes. Geochim Cosmochim Acta 288:176–198

Izawa E, Urashima Y, Ibaraki K, Suzuki R, Yokoyama T, Kawasaki K, Koga A, Taguchi S (1990) The Hishikari gold deposit: high-grade epithermal veins in quarternary volcanics of southern Kyushu, Japan. J Geochem Explor 36:1–56

Jeleň S, Kovalenker VA (1995) Thermodynamic conditions for the formation of Au-Ag base metal mineralization at the Zlatá Baňa deposit. Proceedings of the conference Third geological days of Ján Slávik, Geologický ústav D. Štúra, Bratislava, pp 71–74 (in Slovak)

Kaličiak M (ed) (1991a) Explanations for the geological map of the Slanské Vrchy Mts. And Košická Kotlina depression - northern part 1: 50,000. D. Štúr Institute of Geology, Bratislava. (in Slovak with English summary)

Kaličiak M (ed) (1991b) Geological map of the Slanské Vrchy Mts. and Košická Kotlina depression - northern part 1: 50,000. D. Štúr Institute of Geology, Bratislava

Kaličiak M, Duďa R (1981) Temporal development and formational division of ore mineralization in the Zlatá Baňa ore field. Mineralia Slovaca 13:1–23 (in Slovak)

Kaličiak M, Repčok I (1987) Reconstruction of temporal evolution of volcanoes in the northern part of the Slanské Vrchy Mts. Mineralia Slovaca 19:401–415

Kaufmann A, Lazarov M, Weyer S, Števko M, Kiefer S, Majzlan J (2023) Antimony isotope evolution during hydrothermal precipitation of reduced to oxidized assemblages of antimony minerals in Pezinok (Slovakia). Miner Depos 59:559–757 https://doi.org/10.1007/s00126-023-01222-7.

Koděra P, Šucha V, Lexa J, Fallick AE (2007) The Kremnica Au-Ag epithermal deposit: an example of laterally outflowing hydrothermal system? In: Andrew CJ et al (eds) Digging deeper. Proc 9th SGA Biennial Meeting. Irish Assoc Econ Geol, pp 173–176

Koděra P, Lexa J, Fallick AE, Wälle M, Biroň A (2014) Hydrothermal fluids in epithermal and porphyry Au deposits in the Central Slovakia Volcanic Field. In: Garofalo PS, Ridley JR (eds) Gold-transporting Hydrothermal Fluids in the Earth's Crust. Geol Soc Lond Spec Publ 402:177–206

Kovalenker VA, Jeleň S, Genkin AD, Ďuďa R, Sandomirskaja SM, Malov VS, Kotuľák P (1988) Metallic minerals of productive assemblages of the Zlatá Baňa deposit (Eastern Slovakia); specialities of chemical composition. Mineralia Slovaca 20:481–498

Kraus I, Šamajová E, Šucha V, Lexa J, Hroncová Z (1994) Diagenetic and hydrothermal alterations of volcanic rocks into clay minerals and zeolites (Kremnické Vrchy Mts., the Western Carpathians). Geol Carpath 45:151–158

Kraus I, Chernishev IV, Šucha V, Kovalenker VA, Lebedev VA, Šamajová E (1999) Use of illite for K/Ar dating of hydrothermal precious and base metal mineralization in Central Slovak Neogene volcanic rocks. Geol Carpath 50:353–364

Ledésert BA, Hébert RL, Mouchot J, Bosia C, Ravier G, Seibel O, Dalmais É, Ledésert M, Trullenque G, Sengelen X, Genter A (2021) Scaling in a geothermal heat exchanger at Soultz-Sous-Forêts (Upper Rhine Graben, France): a XRD and SEM-EDS characterization of sulfide precipitates. Geosci 11. https://doi.org/10.3390/geosciences11070271

Lexa J, Halouzka R, Havrila M, Hanzel V, Kubeš P, Liščák P, Hojstričová V (1998) Explanatory notes to the geological map of the Kremnické Vrchy mountain range. Geol Survey of Slovak Rep, Bratislava. (in Slovak with English summary)

Lexa J, Štohl J, Konečný V (1999) Banská Štiavnica ore district: relationship among metallogenetic processes and the geological evolution of a stratovolcano. Min Depos 34:639–665

Lexa J, Bačo P, Bakos F, Baláž P et al (2002) Metallogenetic evaluation of the territory of the Slovak Republic. Final report. Archive of the State Geological Institute of D. Štúr. (in Slovak)

Lobo L, Devulder V, Degryse P, Vanhaecke F (2012) Investigation of natural isotopic variation of Sb in stibnite ores via multi-collector ICP-mass spectrometry – perspectives for Sb isotopic analysis of Roman glass. J Anal Atom Spectrom 27:1304–1310

Lobo L, Degryse P, Shortland A, Eremin K, Vanhaecke F (2014) Copper and antimony isotopic analysis via multicollector ICP-mass spectrometry for provenancing ancient glass. J Anal Atom Spectrom 29:58–64

Majzlan J, Chovan M, Hurai V, Luptáková J (2020) Hydrothermal mineralisation of the Tatric Superunit (Western Carpathians, Slovakia): I. A review of mineralogical, thermometry and isotope data. Geol Carpath 71:85–112

Maťo Ľ, Sasvári T, Bebej J, Kraus I, Schmidt R, Kalinaj M (1996) Structurally-controlled vein-hosted mezothermal gold-quartz and epithermal precious and base metal mineralization in the Banská Hodruša ore field, Central Slovakia neovolcanites. Mineralia Slovaca 28:455–490 (in Slovak)

McKibben MA, Eldridge CS, Reyes AG (1996) Sulfur isotopic systematics of the June 1991 Mount Pinatubo eruptions: a SHRIMP ion microprobe study. In: Newhall CG, Punongbayan R (eds) Fire and mud – eruptions and lahars of Mount Pinatubo, Philippines. Univer Washington, Seattle, pp 825–843

Molnár F, Nagymarosy A, Jeleň S, Bačo P (2010) Minerals and wines: Tokaj Mts., Hungary and Slanské vrchy Mts., Slovakia. Acta Mineralogica-Petrographica, Field Guide Series 15

Morteani G, Ruggieri G, Möller P, Preinfalk C (2011) Geothermal mineralized scales in the pipe system of the geothermal Piancastagnaio power plant (Mt. Amiata geothermal area): a key to understand the stibnite, cinnabarite and gold mineralization of Tuscany (central Italy). Min Depos 46:197–210

Nemčok M, Hók J, Kováč P, Marko F, Madarás J, Bezák V (1993) Tectonics of Western Carpathians during Tertiary (in Slovak). In: Rakús M, Vozár J (eds) Geodynamic model and deep structure of the Western Carpathians. D. Štúr Institute of Geology, Bratislava, pp 263–268. (in Slovak)

Obolensky AA, Gushchina LV, Borisenko AS, Borovikov AA, Pavlova GG (2007) Antimony in hydrothermal processes: solubility, conditions of transfer, and metal-bearing capacity of solutions. Russ Geol Geophys 48:992–1001

Ohmoto H, Rye RO (1979) Isotopes of sulfur and carbon. In: Barnes HL (ed) Geochemistry of hydrothermal ore deposits. John Whiley & Sons, pp 509–561

Olsen NJ, Mountain BW, Seward TM (2018) Antimony (III) sulfide complexes in aqueous solutions at 30°C: a solubility and XAS study. Chem Geol 476:233–247

Olsen NJ, Mountain BW, Seward TM (2019) Antimony (III) speciation in hydrosulfide solutions from 70 to 400°C and up to 300 bar. ACS Earth Space Chem 3:1058–1072

Pécskay Z, Lexa J, Molnár F (2010) Relationships of rhyolite magmatism and epithermal systems in the Central Slovakia and Tokaj Mts. regions of the Western Carpathians: K/Ar dating of volcanic and hydrothermal processes. Acta Miner-Petrogr Abstract Ser 6:297

Pokrovski GS, Borisova AY, Roux J, Hazemann JL, Petdang A, Tella M, Testemale D (2006) Antimony speciation in saline hydrothermal fluids: a combined X-ray absorption fine structure spectroscopy and solubility study. Geochim Cosmochim Acta 70:4196–4214

Reyes AG (1990) Petrology of Philippine geothermal systems and the application on the alteration mineralogy to their assessment. J Volc Geoth Res 43:279–309

Rouxel O, Ludden J, Fouquet Y (2003) Antimony isotope variations in natural systems and implications for their use as geochemical tracers. Chem Geol 200:25–40

Saunders, JA, Unger DL, Kamenov DL, Fayek GD, Hames WE, Utterback WC (2008) Genesis of Middle Miocene Yellowstone hotspot-related bonanza epithermal Au-Ag deposits, Northern Great Basin, USA. Miner Depos 43:715–734

Schwarz-Schampera U (2014) Antimony. In: Gunn G (ed) Critical metals handbook, UK. John Wiley & Sons, Ltd., pp 70–98

Shimizu T (2014) Reinterpretation of quartz textures in terms of hydrothermal fluid evolution at the Koryu Au-Ag deposit, Japan. Econ Geol 109:2051–2065. https://doi.org/10.2113/econgeo.109.7.2051

Shimizu T (2017) Sulfur isotopic ratios and mode of occurrence of stibnite at the Hishikari epithermal Au–Ag deposit. Japan Bull Geol Surv Japan 68:111–117

Shimizu T (2018) Fluid inclusion studies of comb quartz and stibnite at the Hishikari Au–Ag epithermal deposit, Japan. Resour Geol 68:325–335

Sillitoe RH (2015) Epithermal paleosurfaces. Min Depos 50:767–793

Sillitoe RH, Hedenquist JW (2003) Linkages between volcanotectonic settings, ore-fluid compositions, and epithermal precious metal deposits. In: Simmons SF, Graham I (eds) Volcanic, Geothermal,

and Ore-Forming Fluids: Rulers and Witnesses of Processes within the Earth. Econ Geol Spec Publ 10:315–343

Simmons SF, White NC, John D (2005) Geological characteristics of epithermal precious and base metal deposits. In: Hedenquist JW, Thompson JFH, Goldfarb RJ, Richards JP (eds) Economic geology 100th anniversary volume 1905–2005. Soc Econ Geol, Littleton, pp 485–522

Simmons SF, Brown KL, Browne PRL, Rowland JV (2016) Gold and silver resources in Taupo Volcanic Zone geothermal systems. Geothermics 59B:205–214. https://doi.org/10.1016/j.geothermics.2015.07.009

Simpson MP, Mauk JL, Simmons SF (2001) Hydrothermal alteration and hydrologic evolution of the Golden Cross epithermal Au-Ag deposit, New Zealand. Econ Geol 96:773–796

Simpson MP, Palinkas SS, Mauk JL, Bodnar RJ (2015) Fluid inclusion chemistry of adularia-sericite epithermal Au-Ag deposits of the Southern Hauraki Goldfield, New Zealand. Econ Geol 110:763–786

Štohl J, Lexa J, Kaličiak M, Bacsó Z (1994) Metallogeny of stockwork base metal mineralizations in Neogene volcanics of Western Carpathians. Mineralia Slovaca 26:75–117 (in Slovak with English summary)

Tanelli G, Lattanzi P, Ruggieri G, Corsini F (1991) Metallogeny of gold in Tuscany, Italy. In: Ladeira EA (ed) Proc Symp Brazil Gold ´91, Belo Horizonte. Balkema, Rotterdam, pp 109–114

Tanimizu M, Araki Y, Asaoka S, Takahashi Y (2011) Determination of natural isotopic variation in antimony using inductively coupled plasma mass spectrometry for an uncertainty estimation of the standard atomic weight of antimony. Geochem J 45:27–32https://doi.org/10.1007/s00126-023-01187-7

Tharalson ER, Taksavasu T, Monecke T, Reynolds TJ, Kelly NM, Pfaff K, Bell AS, Sherlock R (2023) Textural characteristics of ore mineral dendrites in banded quartz veins from low-sulfidation epithermal deposits: implications for the formation of bonanza-type precious metal enrichment. Miner Depos 58:1395–1419.https://doi.org/10.1007/s00126-023-01187-7

Ueno H, Sawaki T, Kitazono S, Arimura I (2001) Fluid inclusion studies on the epithermal gold deposits in Kagoshima, Japan. In: Piestrzynski A (ed) Mineral deposits at the beginning of the 21st century. Swets & Zeitlinger, Lisse, pp 823–826

Veľký P, Böhmer M, Korim M, Maťo Ľ, Pitoňák P, Oroszlány J, Padúch M, Dimoš I, Verseghy R (1998) Complex evaluation of the precious metal ore deposit Kremnica. Final report. Open file report. Archive of the State Geological Institute of D. Štúr, Bratislava. (in Slovak)

Wang BG, Qin KZ, Song GX, Li GM (2019) A review of intermediate sulfidation epithermal deposits and subclassification. Ore Geol Rev 107:434–456

Wang D, Mathur R, Zheng Y, Qiu K, Wu H (2021) Redox-controlled antimony isotope fractionation in the epithermal system: new insights from a multiple metal stable isotopic combination study of the Zhaxikang Sb-Pb-Zn-Ag deposit in Southern Tibet. Chem Geol 584:120541. https://doi.org/10.1016/j.chemgeo.2021.120541

Wasserman N, Johnson T, Kulp T (2019) Isotopic fractionation of antimony (Sb) during sorption of Sb(III) and Sb(V) to goethite and illite. Goldschmidt Conference Abstracts Barcelona

Wen B, Zhou J, Zhou A, Liu C, Li L (2018) A review of antimony (Sb) isotopes analytical methods and application in environmental systems. Int Biodeterior Biodegrad 128:109–116

William-Jones AR, Normand C (1997) Controls of mineral parageneses in the system Fe-Sb-S-O. Econ Geol 92:308–324

Wilson N, Webster-Brown J, Brown K (2007) Controls on stibnite precipitation at two New Zealand geothermal power stations. Geothermic 36:330–347

Yu HC, Qiu KF, Simon AC, Wang D, Mathur R, Wan RQ, Jiang XY, Deng J (2023) Telescoped boiling and cooling mechanisms triggered hydrothermal stibnite precipitation: insights from the world's largest antimony deposit in Xikuangshan China. Amer Mineral 108:1213–1223

Zhai D, Mathur R, Liu SA, Liu J, Godfrey L, Wang K, Vervoort J (2021) Antimony isotope fractionation in hydrothermal systems. Geochim Cosmochim Acta 306:84–97

Zhou W, Zhou A, Wen B, Liu P, Zhu Z, Finfrock Z, Zhou J (2022) Antimony isotope fractionation during adsorption on aluminum oxides. J Hazard Mater 429:128317. https://doi.org/10.1016/j.jhazmat.2022.128317

Zhou W, Zhou J, Feng X, Wen B, Zhou A, Liu P, Sun G, Zhou Z, Liu X (2023) Antimony isotope fractionation revealed from EXAFS during adsorption on Fe (oxyhydr)oxides. Environ Sci Technol 57:9353–9361. https://doi.org/10.1021/acs.est.3c01906

Zotov AV, Shikina ND, Akinfiev NN (2003) Thermodynamic properties of the Sb (III) hydroxide complex $Sb(OH)_3$ (aq) at hydrothermal conditions. Geochim Cosmochim Acta 67:1821–1836